Validation of the Advanced Microwave Scanning Radiometer for the Earth Observing System (AMSR-E) sea surface temperature in the Southern Ocean

Shenfu Dong,[1] Sarah T. Gille,[1] Janet Sprintall,[1] and Chelle Gentemann[2]

Received 24 February 2005; revised 6 September 2005; accepted 30 December 2005; published 5 April 2006.

[1] Satellite sea surface temperature (SST) measurements from Advanced Microwave Scanning Radiometer for the Earth Observing System (AMSR-E) are compared with in situ temperature observations from high-resolution expendable bathythermograph and hull-mounted thermosalinograph data along two sections (south of Australia and Drake Passage) in the Southern Ocean. To eliminate the effects of diurnal warming and low wind speed, we use only AMSR-E data collected within 5 hours of the in situ observations, with wind speeds exceeding 6 m s^{-1}. The AMSR-E measurements are warmer than in situ observations during summer and are colder than in situ observations during winter. Factors that may cause the temperature difference are examined, including wind speed, columnar water vapor, columnar cloud water, geographic location, local temperature, and time of observation. Of these, wind speed and columnar water vapor are found to be the major factors contributing to the temperature difference between AMSR-E SST and in situ SST observations. The temperature difference decreases with increasing wind speed and water vapor. AMSR-E and in situ SST observations are also compared with simultaneous Moderate Resolution Imaging Spectroradiometer (MODIS) SST and weekly Reynolds Optimum Interpolated (OI) SST. Results suggest that the OI SSTs have a warm bias for both summer and winter; MODIS SSTs indicate a cold bias. In contrast, AMSR-E SSTs show little bias relative to expendable bathythermographs.

Citation: Dong, S., S. T. Gille, J. Sprintall, and C. Gentemann (2006), Validation of the Advanced Microwave Scanning Radiometer for the Earth Observing System (AMSR-E) sea surface temperature in the Southern Ocean, *J. Geophys. Res.*, *111*, C04002, doi:10.1029/2005JC002934.

1. Introduction

[2] Sea surface temperature (SST) has been widely used in studies of climate change and weather forecasting [e.g., *Xie et al.*, 2002; *Sutton and Hodson*, 2003; *Latif et al.*, 2004]. It is a key parameter in the atmospheric and oceanic coupling of heat and momentum and is therefore important for understanding the climate system. The measurement of SST from satellite radiometers has become a major data source for climate research owing to its global coverage and relatively high temporal resolution. Satellite observations are particularly important for Southern Ocean research [e.g., *Moore et al.*, 1999; *O'Neill et al.*, 2005], as in situ observations in the region are sparse and lengthy time series are rare. Given that the Southern Ocean is the only oceanic link between the world's major oceans and plays an important role in the global meridional overturning circulation [*Speer et al.*, 2000], it has the potential to play an important role in global climate.

[3] Several different SST products are produced from a combination of satellite measurements and in situ observations [e.g., *Reynolds et al.*, 2002]. However, infrared measurements are strongly influenced by water vapor and cloud contamination [e.g., *Jones et al.*, 1996; *Merchant and Harris*, 1999; *Vazquez-Cuervo et al.*, 2004], which can cause biases in regions where cloud cover is nearly constant such as the Southern Ocean. This means that studies using infrared SST data in the Southern Ocean must often use composite images at weekly or monthly time intervals. In contrast to infrared radiation, microwave radiation is capable of penetrating through cloud. The Tropical Rainfall Measuring Mission (TRMM) Microwave Imager (TMI) provided the first accurate retrievals of microwave SSTs. Many new features at the ocean surface have been revealed using the TMI data [*Chelton et al.*, 2000]. However, TMI measures SSTs only from 38°N to 38°S. The more recently launched Advanced Microwave Scanning Radiometer for the Earth Observing System (AMSR-E) now provides SSTs for the entire Southern Ocean with twice daily temporal resolution.

[4] Infrared and microwave radiometers measure temperature at slightly different depths in the upper ocean. Because the vertical structure of temperature in the upper few meters of the ocean is complex, the depth at which measurements

[1] Scripps Institution of Oceanography, University of California, San Diego, La Jolla, California, USA.
[2] Remote Sensing Systems, Santa Rosa, California, USA.

0148-0227/06/2005JC002934

are made will significantly impact the value determined for SST. Following classifications developed by *Donlon et al.* [2002] and *Donlon and GHRSST-PP Science Team* [2005], the interface SST is the temperature of an infinitesimally thin layer at the exact air-sea interface; skin SST is a temperature measured by an infrared radiometer at a depth of order 0.01 mm depending on the wavelength of the measurement; subskin SST represents the temperature at the bottom of the skin SST gradient at a depth of approximately 1 mm that corresponds to the attenuation length of microwave radiation; and foundation SST is the temperature free of diurnal temperature variability and is measured traditionally from temperature sensors mounted on ships and buoys at a depth of $\sim 1-5$ m. Foundation SST is similar to previously defined "bulk" SST which is the term used in this study. Two processes, the cool-skin and diurnal warming effects, cause significant differences between the skin and bulk SST measurements. A cool skin layer is almost always present owing to the combined cooling from the net longwave radiation, the latent heat flux, and the sensible heat flux. The nighttime skin-bulk difference is about -0.2°C while the daytime difference may reach several degrees under conditions of low wind speed and high insolation [*Fairall et al.*, 1996a; *Wick et al.*, 1996; *Murray et al.*, 2000]. Studies that make use of data collected using the different measurement techniques must account for differences between skin and bulk temperatures. Both skin and bulk temperatures are important in climate research. Skin SSTs are required to study air-sea interaction [*Fairall et al.*, 1996b], whereas bulk SSTs represent the storage of heat in the upper ocean mixed layer.

[5] The brightness temperature of radiation emitted from the ocean surface is determined by skin SST as well as surface roughness, which in turn depends on wind speed. This radiation is affected by the absorption and emission of water vapor and cloud liquid water in the atmosphere, so brightness temperatures measured by satellites differ from surface measured brightness temperatures [e.g., *Nalli and Smith*, 1998; *Brisson et al.*, 2002; *Merchant and Borgne*, 2004]. In the AMSR-E data, brightness temperatures are corrected for atmospheric effects using the radiative transfer model discussed by *Wentz and Meissner* [1999], where the algorithm constants have been slightly tuned using intercomparison with in situ and climatological observations. In most satellite products, measured brightness temperatures are calibrated against in situ observations and therefore represent subsurface bulk SSTs [e.g., *McClain et al.*, 1985; *Walton*, 1988]. The AMSR-E radiometer was designed to calibrate itself continuously relative to fixed temperatures of hot and cold reference points [*Wentz et al.*, 2003]. Unfortunately, the "hot load" reference temperature does not maintain a constant value. Thus NCEP wind fields and Reynolds OI climatological data are used in combination with the thermistors on the hot load to predict the AMSR-E hot load temperature [see *Wentz et al.*, 2003].

[6] At present, validations of the AMSR-E measurements are mostly based on in situ mooring or buoy data (e.g., the TAO mooring array, surface buoys and drifters) that are collected in the tropics or midlatitudes. Thus the conditions of low water vapor and strong winds with long fetch that are common to higher latitudes are not well represented in the SST validation/calibration process. In this study we present one of the first attempts to evaluate the performance of the AMSR-E microwave temperature at high latitudes using ship-based bulk SST measurements in the Southern Ocean.

[7] Well-calibrated high-resolution expendable bathythermograph and hull-mounted thermosalinograph data from transects of the Drake Passage and south of Australia provide a bulk SST measurement to evaluate the accuracy of AMSR-E subskin SST measurements in the Southern Ocean. In this study, we address the dependence of the difference between these subskin and bulk SSTs on variables such as wind speed, atmospheric water vapor, and cloud liquid water. The data sets used in this study are described in section 2. In section 3 we first compare the AMSR-E SSTs with simultaneous SST measurements from the Moderate Resolution Imaging Spectroradiometer (MODIS). Since Reynolds Optimum Interpolated (OI) SSTs are used in many climate studies, we also compare AMSR-E SST with OI SST. Section 4 presents the evaluation of the AMSR-E measurements, which show that the temperature difference between AMSR-E and in situ SST observations in the Southern Ocean is affected by wind speed and water vapor, even when low-wind-speed data are omitted. Finally, a discussion and summary of the study are given in section 5.

2. Observations

[8] AMSR-E is a multichannel passive microwave radiometer that was launched on NASA's Aqua satellite on 4 May 2002. AMSR-E detects a wide range of geophysical parameters, including SST through cloud, and simultaneous retrievals of wind speed, columnar water vapor, columnar cloud water, rain rate, sea ice and snow. AMSR-E measures the subskin temperature, but it is calibrated and validated with bulk temperature, since in situ subskin SSTs are not routinely collected. Thus we expect that the mean temperature from AMSR-E will match the bulk temperature, although its spatial and temporal variations will be characteristic of the subskin temperature. Version-4 AMSR-E ocean products from http://www.ssmi.com are used in this study without any additional processing. This validation focuses on a two-and-a-half-year period from June 2002 through December 2004. The Aqua satellite is in a sun-synchronous polar orbit, so observations occur at the same local time each day. Equator crossings are at 1430 local time (LT) and 0130 LT, while at 55°S the local crossing times are around 1500 LT and 0100 LT. Data from ascending (local daytime) and descending (local nighttime) portions of the orbit are used separately to examine the day and night difference. In addition, the weekly AMSR-E data are also used to compare with the weekly Reynolds OI SSTs. Both daily and weekly AMSR-E data are on a 0.25° longitude by 0.25° latitude grid.

[9] In situ bulk SST measurements from high-resolution expendable bathythermograph (XBT) and hull-mounted thermosalinograph (TSG) data are used to assess AMSR-E data quality. XBT observations were collected along two repeat lines (Figure 1), one across Drake Passage and the other extending between Hobart, Australia and the French Antarctic base at Dumont d'Urville. The TSG observations for this study are only available along the Drake Passage line. Detailed descriptions of the data were provided by

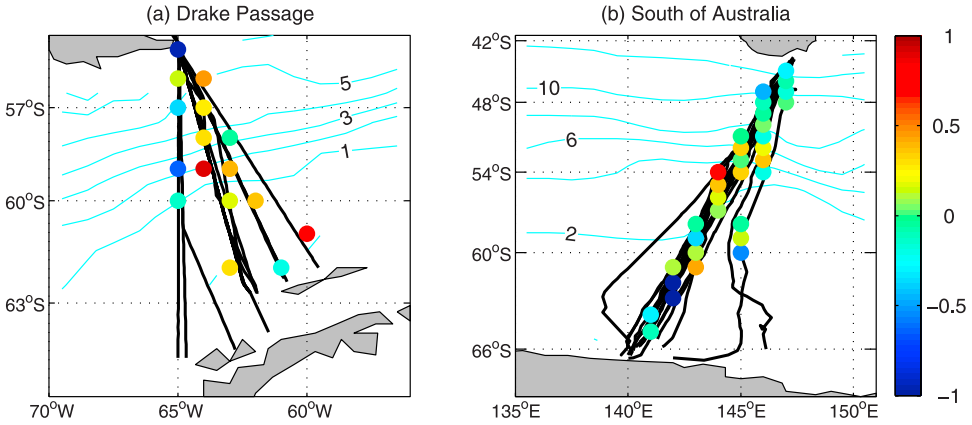

Figure 1. Repeat XBT and TSG lines (black lines) collected in the Southern Ocean between June 2002 and February 2004 for (a) Drake Passage transects and (b) Hobart to Dumont d'Urville transects. The colored dots indicate the mean temperature difference between AMSR-E and XBT at different locations. The color scale is from −1°C (dark blue) to 1°C (red) but actual temperature differences may exceed 1°C in places. Contours indicate mean surface temperatures.

Sprintall [2003] for Drake Passage and by *Morrow et al.* [2003] for south of Australia. During the AMSR-E period, there are a total of 14 transects south of Australia, all carried out during summer (October–March). Along Drake Passage the observations are year round. The TSG is run on every crossing, and XBTs are dropped 6–8 times per year. During the period used in this analysis there are a total of 8 XBT and 15 TSG transects in summer, and in winter 9 XBT and 12 TSG transects. The near surface temperature at 4 m depth is used in this study. The manufactures specify calibration errors of 0.05°C for XBTs and 0.01°C for TSG. However, TSG measurements are 0.15°C warmer than XBT measurements and somewhat noisier. Although the raw 1-min TSG observations were despiked, averaged over 5 min and had a Gaussian filter applied, the TSG temperatures are still relatively noisy. Only data between 51°S and 62°S for the transects south of Australia and between 55°S and 62°S for Drake Passage are used in this study. These latitude ranges were selected in order to exclude shallow water in the north and areas in the south that experience seasonal ice cover.

[10] SST measurements from MODIS, also on the Aqua satellite, are compared with the XBT and AMSR-E SSTs. MODIS SSTs are determined from infrared retrievals of ocean temperature, which are corrected for atmospheric absorption using a combination of several IR bands. Although therefore sensitive to skin SST variability, the MODIS SSTs are calibrated to bulk SST using a match-up database of in situ measurements collected from numerous cruises and buoys. A detailed description of the retrieval algorithm (Katherine A. Kilpatrick, personal communication, 2005) is available from http://modis.gsfc.nasa.gov/data/atbd/ocean_atbd.html. Like other IR measurements, the MODIS measurements of SST are frequently obstructed by cloud, which causes missing data and means that MODIS provides only 35% as many observations as AMSR-E that are close in time to XBT observations. In addition, temperatures may be wrong if clouds are erroneously not detected. The global level-3 mapped thermal IR SST product along with the related statistical and quality files are available from http://podaac.jpl.nasa.gov/. Data with 36 km resolution and with a "good" quality flag are used in this study. No data with "questionable" or "cloudy" flags are used.

[11] Since the Reynolds Optimum Interpolated (OI) SSTs [*Reynolds et al.*, 2002] are commonly used to study climate variations in the global oceans [*McPhaden*, 2004; *Ciasto and Thompson*, 2004], they are also used in this evaluation. OI SSTs are weekly global fields with 1° × 1° resolution derived from satellite IR measurements and in situ SST observations. These data are provided by the NOAA-CIRES Climate Diagnostics Center, Boulder, Colorado, USA, from their web site at http://www.cdc.noaa.gov/.

3. Comparison Between AMSR-E, MODIS, and OI SST

[12] We begin by evaluating the consistency of satellite SST products from AMSR-E, MODIS and OI. Our focus is on the Southern Ocean, so we limit our comparisons to the geographic regions surrounding the in situ XBT observations.

[13] The temporal mean difference between daytime AMSR-E and MODIS temperatures is shown in Figures 2a and 2f along with the temporal mean wind speed (Figures 2b and 2g), water vapor (Figures 2c and 2h) and cloud (Figures 2d and 2i) from AMSR-E for Drake Passage and south of Australia, respectively. The data are simultaneous in time since AMSR-E and MODIS are on the same satellite. Here we have interpolated AMSR-E data onto MODIS grid points for comparison. Results from the nighttime observations (not shown) are similar to those from the daytime. On average, AMSR-E SSTs are warmer than MODIS SSTs in both regions despite the fact that both are calibrated to represent bulk SST. The spatial pattern of the temperature difference (Figures 2a and 2f) corresponds well to the spatial distribution of wind speed (Figures 2b and 2g) both in Drake Passage and south of Australia. The correlation between the two fields is 0.28 in Drake Passage and 0.63 south of Australia, which are above 95% significance level in both regions (0.19). The significance level has been computed to account for the autocorrelation length scales of the maps, which are 1 degree in latitude and 1 degree in longitude in the

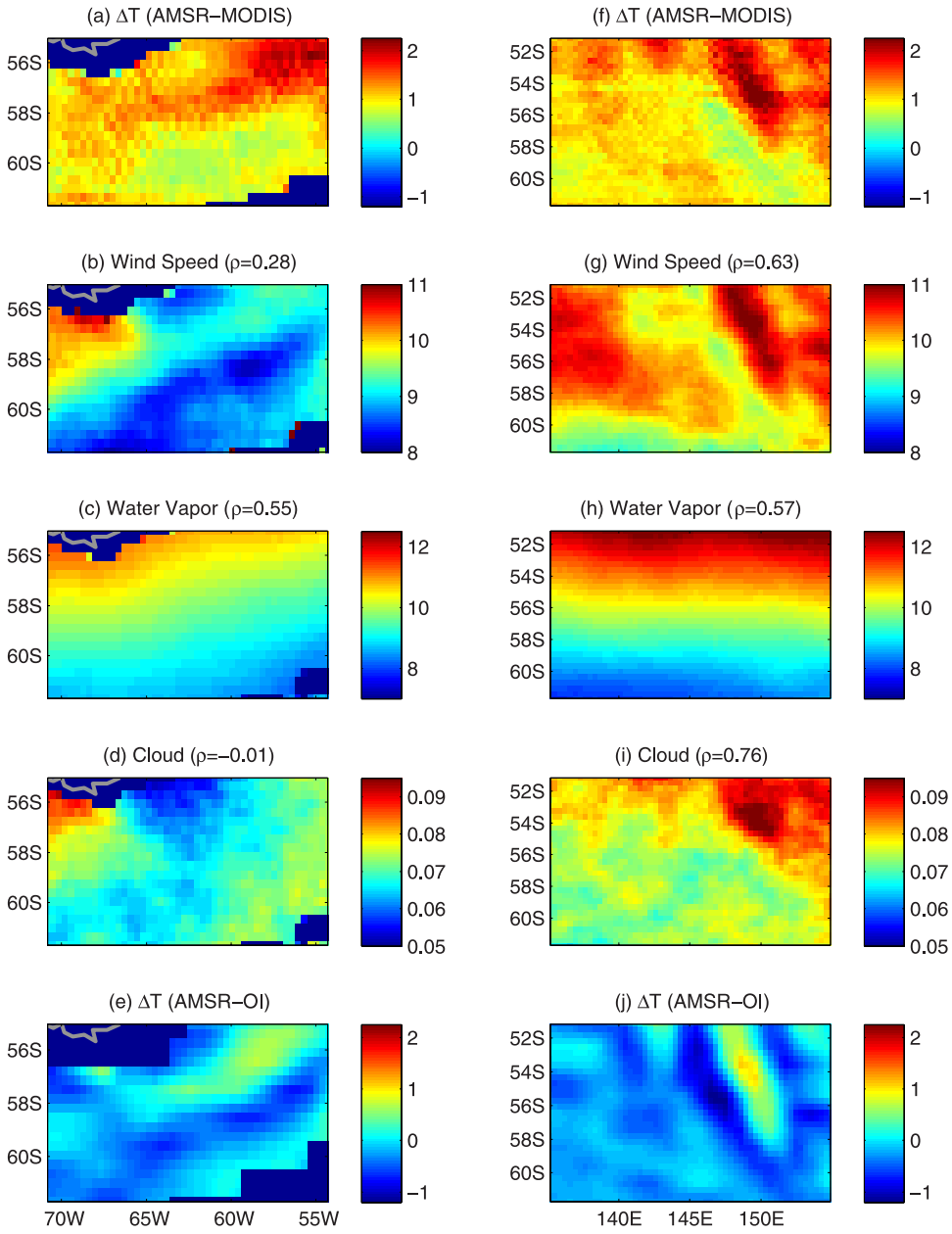

Figure 2. Spatial distribution of the temporal mean (a) temperature difference between AMSR-E and MODIS, (b) wind speed, (c) columnar water vapor, (d) columnar cloud water, and (e) temperature difference between AMSR-E and Reynolds OI SST in the Drake Passage region. (f, g, h, i, j) Same as Figures 2a–2e but for the region south of Australia. Here ñ is the correlation between temperature difference (AMSR-E and MODIS) and wind speed, water vapor, and cloud, respectively. The 95% significance level is 0.19 for both regions.

Drake Passage, and 1 degree in latitude and 2 degrees in longitude in the region south of Australia. As noted above, the roughness of the ocean surface, which is affected by wind speed, has a large influence on microwave emission and this may account for some of the spatial distribution in the temperature difference. The temperature difference is also significantly correlated with water vapor (Figures 2c and 2h). For the region south of Australia, the spatial pattern of the temperature difference also corresponds to cloud distribution (Figure 2i). This suggests that although all spurious data flagged as being cloud contaminated were removed prior to this analysis, some undetected cloud contamination may remain in the MODIS measurements. Since wind speed, water vapor, and cloud all influence microwave brightness temperature, these effects could potentially contaminate SST estimates. This may account for some of the correlation between these geophysical parameters and the temperature difference (AMSR-E minus MODIS). However, *Wentz and Meissner* [1999] suggested that this effect should be minimal.

[14] We also compare AMSR-E and MODIS SSTs nearest in time to the XBT observations. Unlike the cloud-free AMSR-E measurements, MODIS SSTs are not always available at the time of the XBT observations owing to

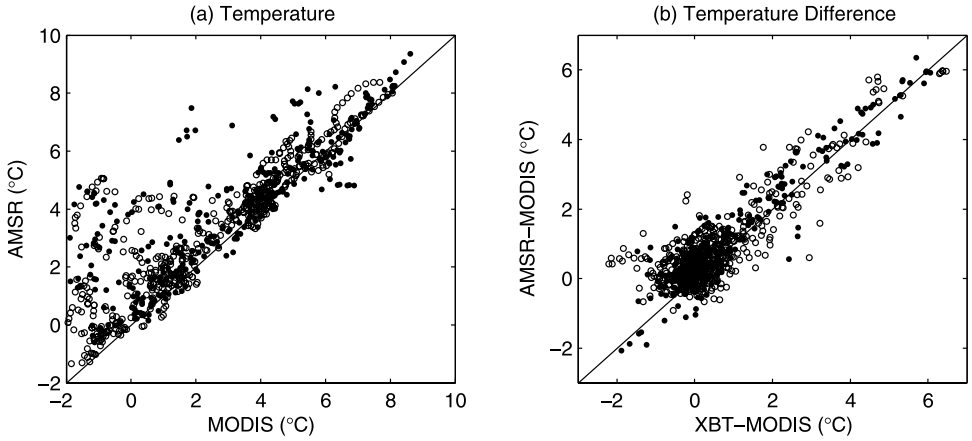

Figure 3. Scatterplots of (a) sea surface temperature from AMSR-E against that from MODIS and (b) temperature difference between AMSR-E and MODIS against that between XBT and MODIS. All available data from the Drake Passage transects (circles) and the transects between Hobart and Dumont d'Urville (dots) are included in the figure.

cloud cover. Over the two-and-a-half-year time period, we found fewer than 300 simultaneous AMSR-E and MODIS observations on the same day as the ~1400 XBT observational times along both transects.

[15] A scatterplot (Figure 3a) of MODIS SSTs versus AMSR-E SSTs shows that the two measurements are comparable most of the time, but a number of data deviate substantially from the zero bias line (at a 45° angle relative to the *x* axis). The large scatter is due to either cold MODIS biases or warm AMSR-E biases. Comparison of SST difference from (AMSR-E - MODIS) versus (XBT - MODIS) in Figure 3b shows that the MODIS SSTs differ from both the AMSR-E and XBT SSTs, suggesting that MODIS observations are biased cold. Fortunately, 86% of the temperature differences in Figure 3b are concentrated within ±2°C, so for subsequent analyses we exclude the MODIS data that differ from the nearest XBT observations by more than 2°C. However, even after removing the extremely spurious MODIS data, MODIS SSTs are still cold compared to AMSR-E SSTs along both transects: −0.56 ± 0.03°C at the Drake Passage, and −0.39 ± 0.04°C south of Australia. These cold biases could be due to residual cloud contamination in the MODIS measurements.

[16] The blended OI SST product derived from the Advanced Very High Resolution Radiometer (AVHRR) in combination with in situ observations has been used in many climate studies. An improved version of OI SST with small global residual biases of −0.03°C was developed by *Reynolds et al.* [2002]. They pointed out that the midlatitude Southern Hemisphere (60°S–30°S) is the major contributor to this residual negative bias in the OI SST owing to the sparse number of in situ observations in this region. We examine whether AMSR-E measurements are biased relative to OI SSTs.

[17] Comparisons of OI SSTs with both daily and weekly AMSR-E data give similar results. Thus, unless otherwise specified, the results shown here are compared with weekly AMSR-E. *Wentz et al.* [2003] examined the difference between AMSR-E SST retrievals and Reynolds OI SST. They attributed part of the difference to the low spatial and temporal resolution of the Reynolds product, which smoothes out the sharp frontal structure shown in AMSR-E and XBT SSTs (Figure 4). This results in the high-low-high pattern of the mean temperature difference between the two products in the Drake Passage region (Figure 2e) and in the region of south of Australia (Figure 2j). Surprisingly, the spatial pattern of the temperature difference between AMSR-E and OI SSTs (Figures 2e and 2j) resembles that between AMSR-E and higher resolution MODIS SSTs (Figures 2a and 2f), although the patterns differ in magnitude. The consistent spatial distribution suggests that the difference between AMSR-E and Reynolds OI SSTs may not be due entirely to the low resolution of the Reynolds OI product. The influence of geophysical parameters on the measurements, such as the effects of wind speed on microwave emission and cloud contamination of IR radiation, may also explain some of the high-low-high pattern of the temperature difference.

[18] Over the Southern Ocean (30°S–60°S) for the two-and-a-half-year period considered here, the spatial-temporal mean AMSR-E SST is 0.08°C cooler than the OI SSTs. This negative difference could be due to either a cold bias in AMSR-E SSTs or to a warm bias in the OI SSTs. These possibilities will be examined using in situ observations in section 4.

4. Comparison Between AMSR-E and XBT/TSG

[19] In this section, we focus on the comparison between AMSR-E measurements and in situ observations and also provide a brief comparison of MODIS and OI SSTs to XBT observations. Here the AMSR-E data from local daytime (ascending) and local nighttime (descending) observations are separately compared to the bulk SSTs measured by the XBTs, in order to examine the day and night difference. The AMSR-E measurements nearest in time to the XBT and TSG observations are interpolated to the XBT and TSG locations. Figure 4 shows an example of the temperature distribution along both lines. Spatial structures shown in the XBT observations are well captured by the AMSR-E measurements. Although the Reynolds OI SST in Figure 4 shows the large-scale structure, it cannot capture the detailed structure owing to its low spatial resolution.

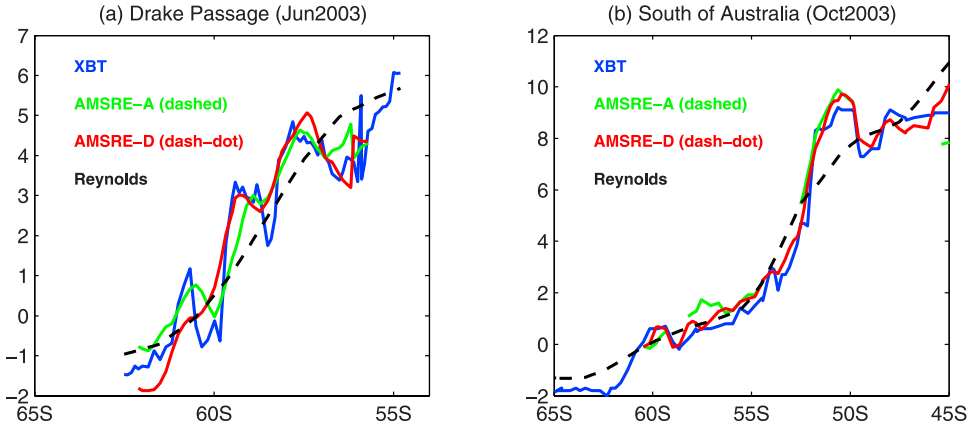

Figure 4. Examples of the sea surface temperature (a) across Drake Passage and (b) between Hobart and Dumont d'Urville as a function of latitude. The four different SSTs are from XBT (blue), ascending AMSR-E (green), descending AMSR-E (red), and Reynolds (black), respectively.

[20] The temperature difference, ΔSST defined as AMSR-E minus XBT/TSG, is examined to evaluate how well the AMSR-E temperatures in the Southern Ocean are calibrated. As mentioned in section 2, the spatial and temporal variability of the AMSR-E SST are likely characteristic of subskin SST. Thus ΔSST will include both spatial patterns associated with the subskin-bulk difference and any algorithm errors. In the following analysis, we examine potential temperature differences caused by the time separation between the AMSR-E and XBT/TSG observations, the effect of low wind speeds and other geophysical parameters.

4.1. Time-of-Day Effect

[21] SST varies with the diurnal cycle of solar insolation. Under conditions with light or moderate winds, the trapping depth of the thermal response is typically O(10 m) [*Price et al.*, 1986]. Unfortunately, because of the nature of the continuous underway sampling of the XBT/TSG observations on bimonthly cruises we are unable to evaluate diurnal cycles from these measurements. However, the TRMM satellite is not on a sun-synchronous orbit, and its TMI SST measurements from this satellite resolve the complete diurnal cycle within a 23-day period. Examination of the TMI measurements [*Gentemann et al.*, 2003] suggests that diurnal warming starts at 0800 LT and peaks at 1500 LT. The warming then decays gradually until 2300 LT with little variability afterward (from 0100 LT to 0800 LT). The diurnal cycle from the TMI measurements may not represent that at high latitudes. In addition, owing to the large seasonal variations in solar insolation at high latitude, in the Southern Ocean we would expect the daily cycle in SST during summer to differ from that during winter. However, we use the diurnal cycle from TMI measurements as a reference in our analysis.

[22] XBT and TSG data on any one transect are collected continuously throughout the day and night, while AMSR-E measurements are made only at the specific times of satellite overpasses. The time separation in the two data sets may contribute to the ΔSST owing to the magnitude of diurnal warming. Figure 5 shows a schematic diagram of the expected ΔSST (temperature at a fixed time minus the

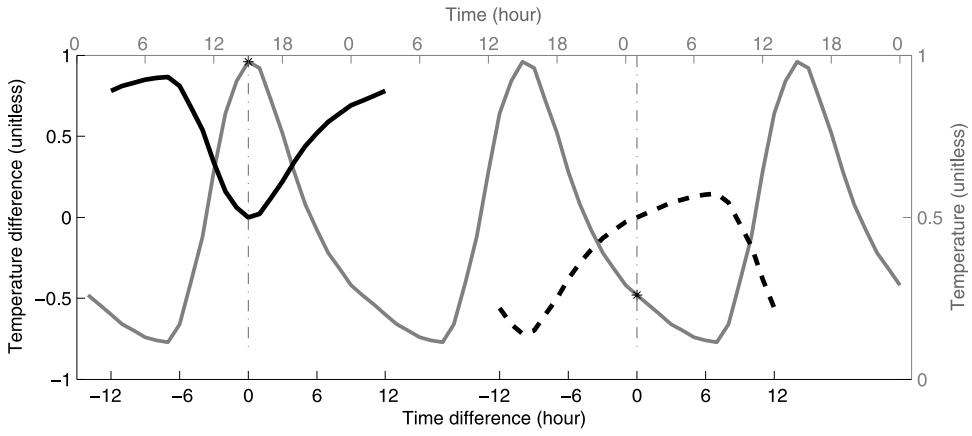

Figure 5. Schematic diagram of expected ΔSST with increasing time separation from fixed time of 0100 local time (LT) (nighttime, black dashed line) and 1500 LT (daytime, black line) which corresponds to the AMSR-E satellite local crossing time in the Southern Ocean. The ΔSST at a given time separation (lower axis) is the temperature at the fixed times (stars) minus the expected temperature from the diurnal cycle (gray line) at that time (upper axis).

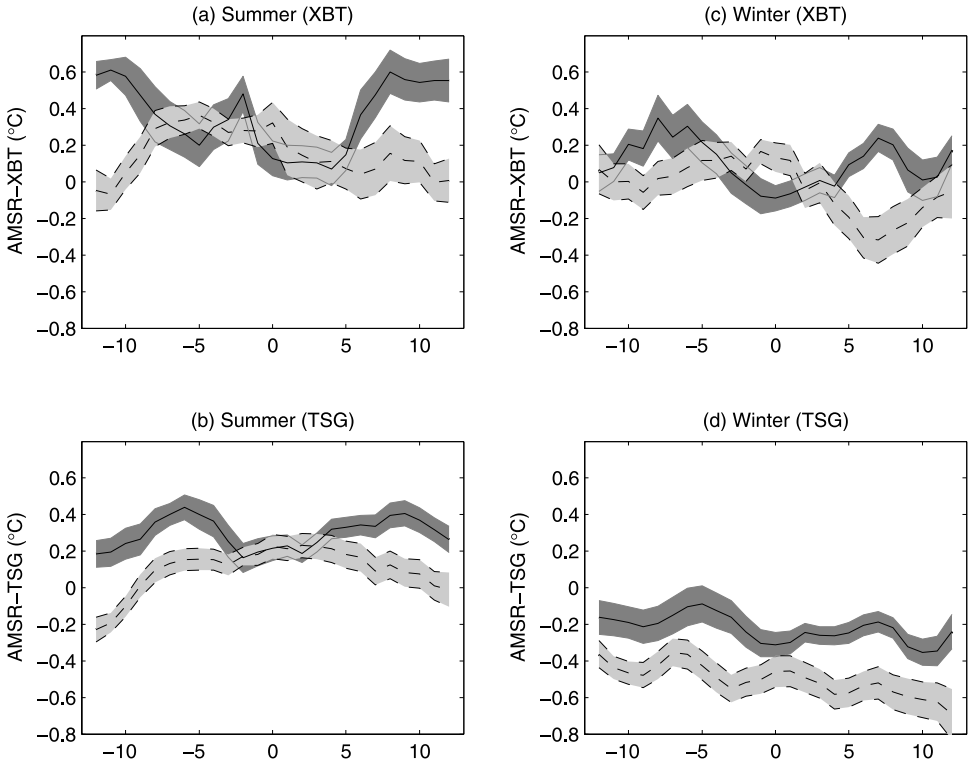

Figure 6. Changes of temperature difference (AMSR-E minus XBT) with increasing time separation for Drake Passage transects in (a) summer and (c) winter. The lines (daytime, solid line; nighttime, dashed line) indicate the temperature difference and the shading area shows the standard error. (b, d) Same as Figures 6a and 6c, respectively, but for the temperature difference between AMSR-E and TSG.

diurnal cycle) relative to the time difference from the satellite overpass. The AMSR-E daytime measurements occur at about 1500 LT for both sections, which is probably close to the peak of the diurnal cycle [*Gentemann et al.*, 2003, 2004]. Under the condition that AMSR-E SSTs match simultaneous XBT/TSG measurements, the ΔSSTd (daytime AMSR-E minus XBT/TSG) should be close to zero for the XBT/TSG SSTs measured at 1500 LT (zero time lag) and should increase with increasing time separation. The maximum ΔSSTd occurs when the XBT/TSG observations are at 0800 LT because AMSR-E and XBT/TSG measure the warm and cold phase of the diurnal cycle, respectively. In contrast, the nighttime (0100 LT) measurements are during the period when *Gentemann et al.* [2003] found little SST variability. The ΔSSTn (nighttime AMSR-E minus XBT/TSG) should be close to zero for the XBT/TSG observations at 0100 LT and very small within a few hours, but should then decrease (becoming more negative) with increasing time separation. The ΔSSTn reaches its most negative values for the XBT/TSG observations at 1500 LT.

[23] Simple scatterplots (not shown) of ΔSST against time separation do not show any apparent relationship. To examine the relationship more carefully, we bin averaged ΔSST by time separation. Data with wind speeds less than 6 m s^{-1} are not included in this calculation because ΔSST depends strongly on wind speed, particularly under low wind conditions, as discussed in section 4.2. Figures 6 and 7 show the changes of the mean ΔSST with increasing time separation for Drake Passage XBT transects and XBT transects between Hobart and Dumont d'Urville, respectively. As illustrated in Figure 5, we would expect daytime ΔSST to become more positive and nighttime ΔSST to become more negative with increasing time separation. The results shown in Figures 6 and 7 indeed are consistent with this expectation, though ΔSST is not zero at zero time lag. The mean ΔSST from summer daytime and nighttime tracks are nearly constant within a few hours of separation for all cases. However, during winter, the ΔSST at zero time lag from daytime tracks differ from nighttime tracks.

[24] The trends with increasing time separation for both daytime and nighttime tracks suggest that the diurnal signal in SST affects ΔSST. Figure 6 indicates that ΔSST is not significantly different for time separations less than 5 hours. This is also shown in Figure 7, though there is a relatively large change in ΔSST when the time of XBT observations leads the AMSR-E measurements by about 3 hours. Both Figure 6 and Figure 7 suggest a diurnal variation in temperature as suggested schematically in Figure 5. To eliminate the diurnal effect and retain as much data as possible, in the following analysis, unless otherwise specified, we employ data with time separations of no more than 5 hours.

4.2. Low-Wind-Speed Effect

[25] Previous studies [*Murray et al.*, 2000; *Donlon et al.*, 2002; *Gentemann et al.*, 2004] found that the temperature difference between skin and bulk had large variations at low wind speed. Stronger wind tends to mix the water column, causing small skin-bulk SST differences. Under weak wind conditions, especially during the daytime with solar insola-

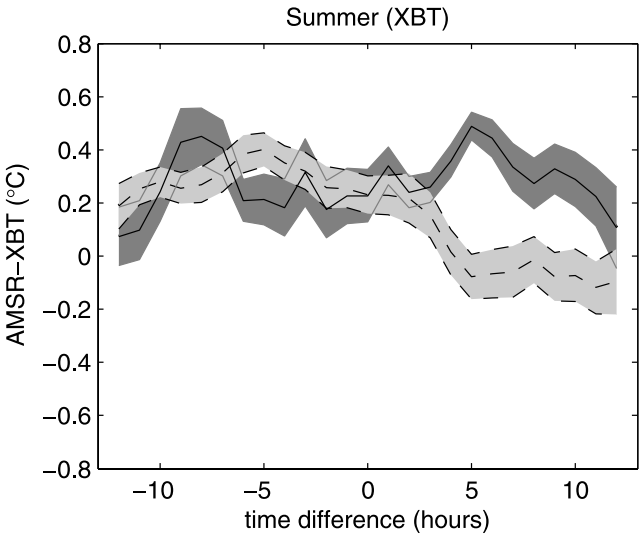

Figure 7. Same as Figure 6 but for summertime transects between Hobart and Dumont d'Urville.

tion, skin-bulk SST differences tend to be larger. Our analysis indicates that the relationships between ΔSST and wind speed are statistically consistent for the two sections and for XBT and TSG in situ observations, so data from the two sections and from XBT and TSG are combined in the following analysis.

[26] ΔSST decreases rapidly with increasing wind speed until 5–6 m s^{-1} for summer daytime (Figure 8a). The largest ΔSST, about 2.7°C, occurs at low wind speed. During the summer nighttime (Figure 8b), ΔSST reaches about 1°C at low wind speed. Table 1, which compares the mean and standard error of ΔSST for summer and winter, daytime and nighttime, and for cases with and without low-wind-speed data, shows that ΔSST decreases significantly for summer daytime measurements after removing low-wind-speed data. The change in ΔSST (Table 1) is insignificant during winter owing to higher wind speeds and low solar insolation, and also during summer nighttime when the near-surface stratification is weak owing to lack of solar insolation. Although the low-wind-speed effect partly explains the warm ΔSST during summer daytime (Table 1), it cannot explain the warm AMSR-E SST during summer nighttime (Table 1), when solar insolation is absent but

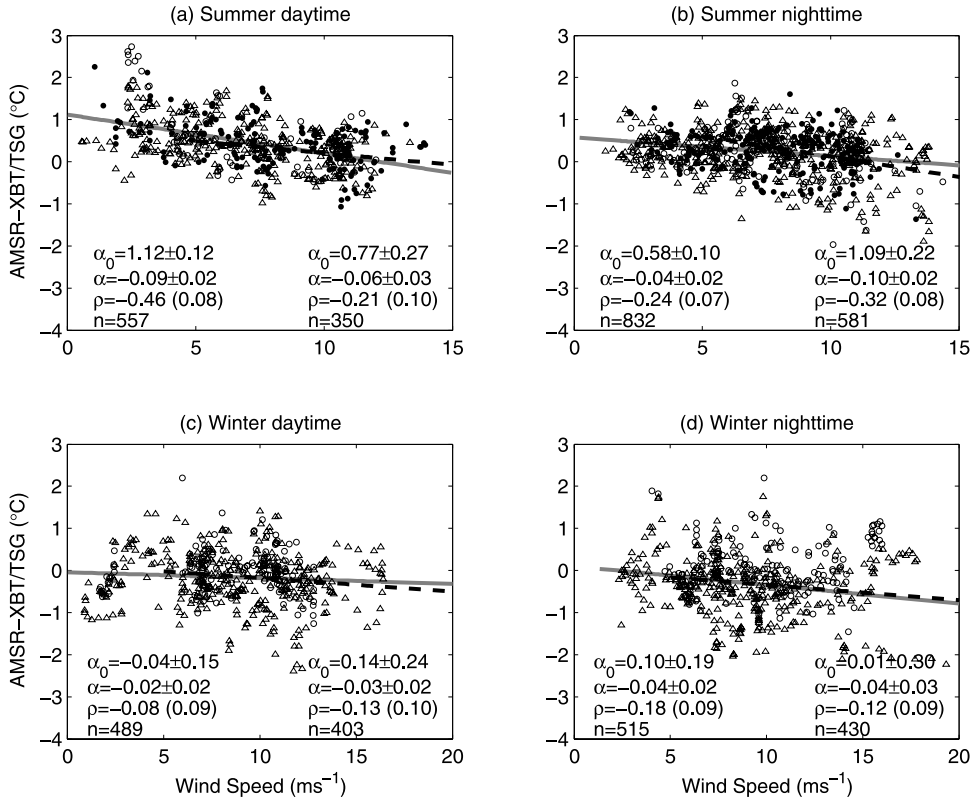

Figure 8. Scatterplots of temperature difference against wind speed for (a) summer daytime, (b) summer nighttime, (c) winter daytime, and (d) winter nighttime. Dots represent transects between Hobart and Dumont d'Urville and circles represent Drake Passage transects for AMSR-E minus XBT, and triangles are AMSR-E minus TSG for Drake Passage transects. The gray (all data) and dashed black (data with wind speeds exceeding 6 m s^{-1}) lines are the linear regression of temperature difference to wind speed, $\Delta SST = \acute{a}_0 + \acute{a}W$. The regression coefficients, number of data points (n), and correlation coefficient (ñ) between ΔSST and wind speed are listed in the figure. The value in parentheses indicates the corresponding 95% significance level of the correlation. Variables on the left correspond to all data, and those on the right correspond to data with wind speeds exceeding 6 m s^{-1}.

Table 1. Temporal Mean Temperature Difference Between AMSR and XBT/TSG and the Corresponding Standard Error for Winter and Summer, Daytime and Nighttime, Separately[a]

Location	Parameters	AMSR - XBT	AMSR - TSG
	Summer		
South of Australia	ascending (daytime)	0.42 ± 0.05	
	wind speed ≥ 6 m s^{-1}	*0.28 ± 0.05*	
	wind speed < 6 m s^{-1}	*0.83 ± 0.08*	
	descending (nighttime)	0.26 ± 0.03	
	wind speed ≥ 6 m s^{-1}	*0.23 ± 0.04*	
	wind speed < 6 m s^{-1}	*0.37 ± 0.05*	
Drake Passage	ascending (daytime)	0.57 ± 0.09	0.42 ± 0.03
	wind speed ≥ 6 m s^{-1}	*0.21 ± 0.06*	*0.24 ± 0.04*
	wind speed < 6 m s^{-1}	*1.08 ± 0.15*	*0.68 ± 0.04*
	descending (nighttime)	0.24 ± 0.04	0.23 ± 0.03
	wind speed ≥ 6 m s^{-1}	*0.24 ± 0.06*	*0.19 ± 0.04*
	wind speed < 6 m s^{-1}	*0.26 ± 0.04*	*0.30 ± 0.03*
	Winter		
Drake Passage	ascending (daytime)	−0.03 ± 0.05	−0.21 ± 0.03
	wind speed ≥ 6 m s^{-1}	*−0.01 ± 0.05*	−0.24 ± *0.04*
	wind speed < 6 m s^{-1}	*−0.13 ± 0.16*	*−0.09 ± 0.08*
	Descending (nighttime)	0.07 ± 0.05	−0.42 ± 0.04
	wind speed ≥ 6 m s^{-1}	*0.08 ± 0.05*	*−0.51 ± 0.04*
	wind speed < 6 m s^{-1}	*−0.09 ± 0.17*	*−0.08 ± 0.07*

[a]Results from three different cases (all available data, data with wind speed greater than 6 m s^{-1}, and data with wind speed less than 6 m s^{-1}) are listed.

radiative cooling is dominant. ΔSST is regressed to wind speed (gray lines in Figure 8), the regression coefficients are statistically different from zero, suggesting a dependence of ΔSST on wind speed. Similarly, the correlations between ΔSST and wind speed all exceed the 95% significance level (Figure 8). The low-wind-speed effect explains the relatively high correlation and large slope of the regression during summer daytime (Figure 8a).

[27] The low-wind-speed effect on ΔSST is consistent with the results from comparisons of TMI and buoy data in the tropics [*Gentemann and Wentz*, 2001; *Gentemann et al.*, 2004]. *Gentemann et al.* [2004] also found a weak cooling during the nighttime at wind speeds less than 1 m s^{-1}, when wind-driven convective overturning ceases and radiative cooling becomes the dominant mechanism. Since the wind speed along the Southern Ocean XBT transects always exceeds 1 m s^{-1} during nighttime (Figures 8b and 8d), we are unable to examine the radiative cooling effect at very low wind speed. Nighttime data (Figures 8b and 8d) indicate that ΔSST levels off for wind speed lower than 5–6 m s^{-1}, which may be owing to the cool-skin effect.

[28] The decoupling between skin and bulk SSTs at wind speeds lower than 6 m s^{-1} [*Donlon et al.*, 1999, 2002] due to the surface stratification and cool-skin effects makes it difficult to compare the skin and bulk SSTs. *Donlon et al.* [1999] suggested that variability in ΔSST is diminished in all cases for wind speeds larger than 6 m s^{-1}. Our data shown in Figure 8 do not support their conclusion. The dependence of ΔSST on wind speed is apparent for wind speeds larger than 6 m s^{-1}. However, for consistency with previous studies [*Murray et al.*, 2000; *Donlon et al.*, 2002; *Gentemann et al.*, 2004] to examine the relationship between ΔSST and different geophysical parameters, in this study we focus on the data collected when wind speeds exceeded 6 m s^{-1}. The relationship between ΔSST and wind speed larger than 6 m s^{-1} will be further examined in section 4.4.

4.3. Seasonal Differences

[29] Figures 9 and 10 show scatterplots of AMSR-E subskin SST against bulk SST from XBT and TSG measurements, sorted by season. All available data with wind speeds exceeding 6 m s^{-1} that were collected within 5 hours of the in situ observations are used, with daytime observations shown as dots and nighttime observations as circles. The data scatter along the zero bias line, demonstrating that the two data sets agree fairly well, although the AMSR-E measurements tend to be warmer than the XBT/TSG observations during summer and cooler than the XBT/TSG observations during winter. The seasonal and diurnal differences in mean ΔSST are given in Table 1. For both XBT sections, the AMSR-E SST has a warm bias of ∼0.24°C during summer. During winter, the daytime AMSR-E SST at the Drake Passage does not significantly differ from the XBT SST and the nighttime AMSR-E SST has a weak warm bias of 0.08°C. The lower ΔSST during winter compared to summer may be due to the seasonal differences in solar insolation at high latitudes as well as the lack of low-wind-speed events during winter. Thus the strong bias at low wind speed is a summer-only phenomenon. The winter TSG data are 0.24°C warmer than AMSR-E during the day and 0.51°C warmer at night, possibly owing to the warm bias of TSG observations mentioned in section 2.

[30] *Stammer et al.* [2003] found seasonal cycles in the temperature difference between TMI SST and XBT data at midlatitudes of the same sense that we find here. They suggested that the seasonal cycle could be caused by the shallow mixed layer depth and large near-surface stratifications during summer due to solar insolation. In light of the seasonal differences, the analysis that follows considers winter and summer separately.

4.4. Evaluation of the AMSR-E

[31] The dependence of ΔSST on the simultaneous retrievals of wind speed, cloud liquid water, and columnar water vapor are examined in this subsection. We also examine the potential dependence of ΔSST on the geographic location, local time, and local temperature. Our examination suggests that the relationship between ΔSST and geophysical parameters are not statistically different for the two XBT sections and for XBT and TSG observations. Thus we combine data from both sections and from XBT and TSG together for the following analysis, but separate them into summer and winter.

[32] Even after excluding AMSR-E data collected at low wind speed or separated by more than 5 hours from the in situ XBT/TSG observations, we still find a residual bias between AMSR-E and the in situ temperatures (Table 1). As noted above, biases can represent either algorithm problems or physical differences between skin temperatures measured by the satellite and bulk temperatures from the in situ XBT/TSG measurements. We consider a number of possible explanations for this bias.

[33] First, although the microwave radiometer has the capability to retrieve SST through clouds, we considered the possibility that cloud liquid water might influence the

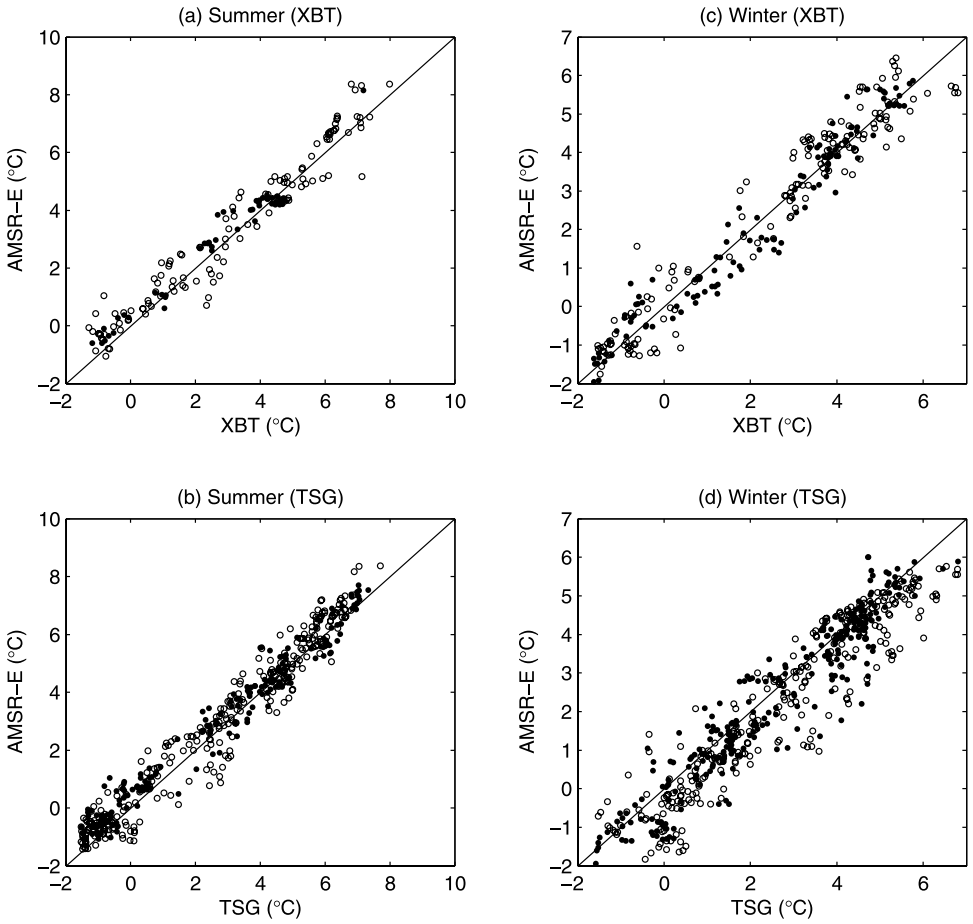

Figure 9. Scatterplots of sea surface temperature from XBT/TSG (x axis) against that from daytime AMSR-E (dot) and nighttime AMSR-E (circle) for (left) summer and (right) winter for Drake Passage transects.

retrievals. However, in agreement with findings for TMI SSTs [*Gentemann et al.*, 2004], we found that ΔSST and AMSR-E cloud liquid water were not correlated at the 95% significance level.

[34] Second, although we excluded the low-wind-speed data (<6 m s^{-1}) as suggested by previous studies [*Donlon et al.*, 1999, 2002; *Gentemann et al.*, 2004], we explored the dependence of ΔSST on wind speed. In Figure 8, ΔSST is regressed to wind speed (dashed black lines). The statistical analyses suggest that ΔSST has a significant dependence on wind speed for both summer and winter for wind speeds exceeding 6 m s^{-1}, though the dependence in summer (Figures 8a and 8b) is stronger than that in winter (Figures 8c and 8d). During summer, at low wind speeds, ΔSST (Figures 8a and 8b) is positive, it decreases to zero as wind speeds increase to ~10 m s^{-1}, and it becomes negative at larger wind speeds. The wintertime ΔSST (Figures 8c and 8d) is more negative as indicated by the regression, and decreases with increasing wind speed. This suggests that in the Southern Ocean, ΔSST is still significant at wind speeds exceeding 6 m s^{-1}, while at lower latitudes this dependence only occurs at wind speeds less than 6 m s^{-1} [*Donlon et al.*, 1999, 2002; *Gentemann et al.*, 2004]. The negative ΔSST at wind speeds above 12 m s^{-1} (Figures 11a and 11c) is consis-

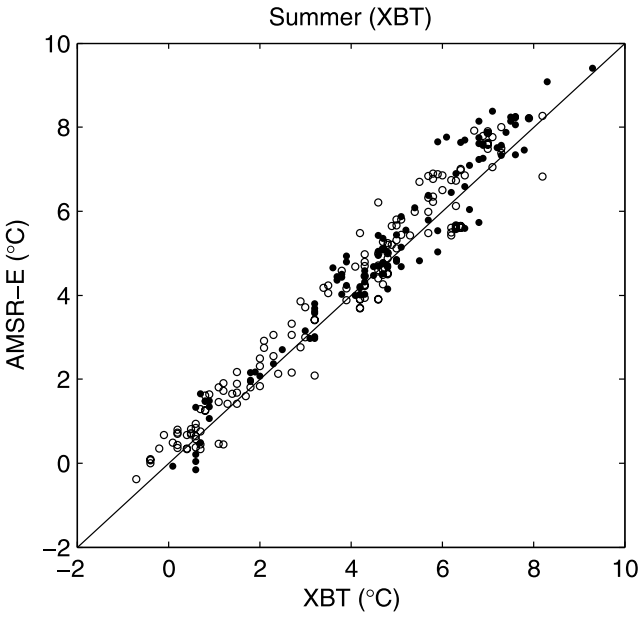

Figure 10. Same as Figure 9 but for summertime transects between Hobart and Dumont d'Urville.

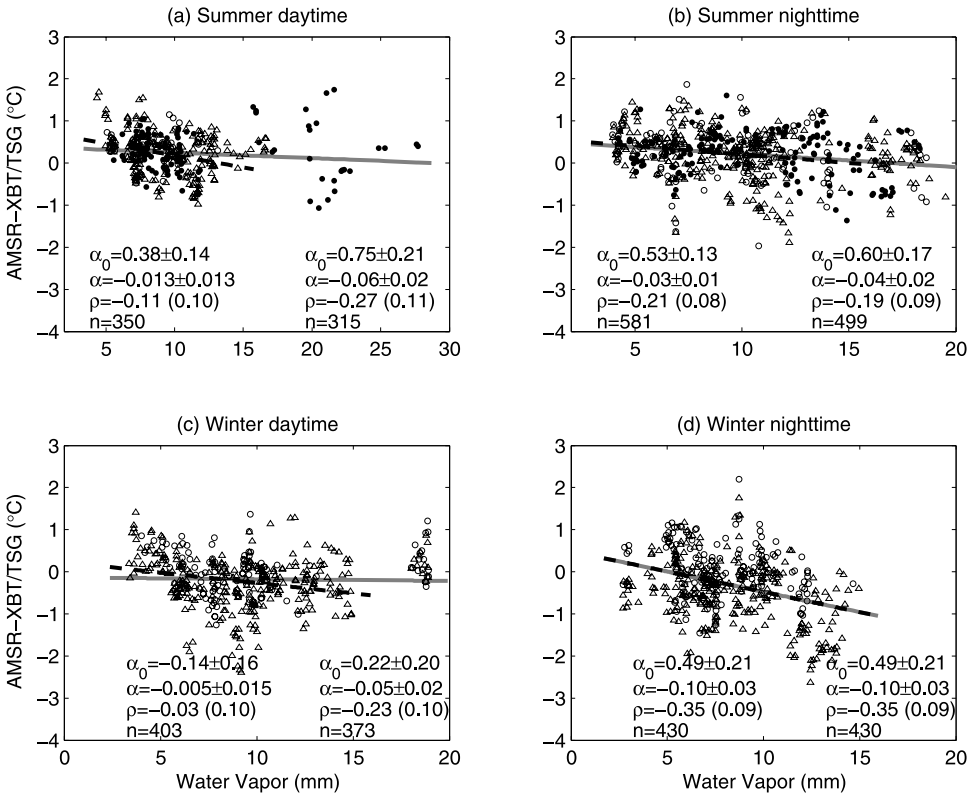

Figure 11. Scatterplots of temperature difference against atmospheric water vapor for (a) summer daytime, (b) summer nighttime, (c) winter daytime, and (d) winter nighttime. The gray (all data) and dashed black (data with water vapor less than 15 mm) lines are the linear regression of temperature difference to water vapor, $\Delta SST = \acute{a}_0 + \acute{a}V$. Variables on the left correspond to all data, and those on the right correspond to the data with water vapor less than 15 mm. Dots indicate data from the XBT transects between Hobart and Dumont d'Urville, and circles (XBT) and triangles (TSG) are for data from the Drake Passage transects.

tent with the cool bias also found in the TMI SSTs at higher wind speeds [*Gentemann and Wentz*, 2001]. Comparing the gray and the dashed black lines in Figure 8b, it is evident that the slope of the regression for nighttime is increased when the low-wind-speed data are excluded, which is consistent with a strong cool-skin effect at low wind speed. The dependence of ΔSST on higher wind speed could be explained by errors in the calibration at high latitudes. Wind velocity, wind direction, and wind fetch all affect sea surface roughness [*Yoshimori et al.*, 1994] which, in turn, leads to high sea surface emissivity. The longer fetch of the wind in the Southern Ocean may not be properly represented in the retrieval algorithm, nor in the calibration because of the lack of in situ observations, which may cause a bias in the SST.

[35] *Gentemann et al.* [2004] found that the columnar water vapor does not affect ΔSST. However, our regression (Figure 11) suggests that ΔSST decreases with increasing water vapor at a rate of 0.03°C mm^{-1} in summer nighttime and 0.1°C mm^{-1} in winter nighttime. ΔSST does not show significant dependence on water vapor during daytime (Figures 11a and 11c, gray lines), but the regression is controlled by the few data with high water vapor. If we exclude data with water vapor above 15 mm, the regression analysis (dashed black lines in Figure 11) shows consistent results for daytime and nighttime. The dependence of ΔSST on water vapor suggests that there is a calibration problem for AMSR-E SST retrievals in the Southern Ocean. One potential explanation is the difference in water vapor content between high and low latitudes. The water vapor in our study region is often less than 20 mm whereas in low latitudes it is often higher than 20 mm. As shown in Figure 11, ΔSST decreases with increasing water vapor, and hence it is possible that ΔSST is not significant for high water vapor cases. The water vapor absorption is calibrated using radiosonde observations. In comparison to low latitudes, at higher latitudes there are fewer calibration data, which may lead to a poorer calibration under low water vapor conditions.

[36] *Gentemann et al.* [2004] found that the difference between TMI and buoy temperatures at high wind speed (5–10 m s^{-1}) varies with local time. TMI SSTs are colder than buoy SSTs during daytime (1100 LT to 1800 LT) and are warmer than buoy SSTs during nighttime with an overall zero mean difference [*Gentemann et al.*, 2004, Table 1]. They attributed the diurnal variability of the difference to an imperfect correction for the oxidation of the primary TRMM antenna. Time dependence is more difficult to examine from AMSR-E's twice-daily measurements. However, the mean daytime and nighttime ΔSST are not significantly different after removing the low-wind-speed effect, except in the comparison with wintertime TSG observations. This suggests that the AMSR-E measurements do not have the oxidation-correction problem found in TMI measurements.

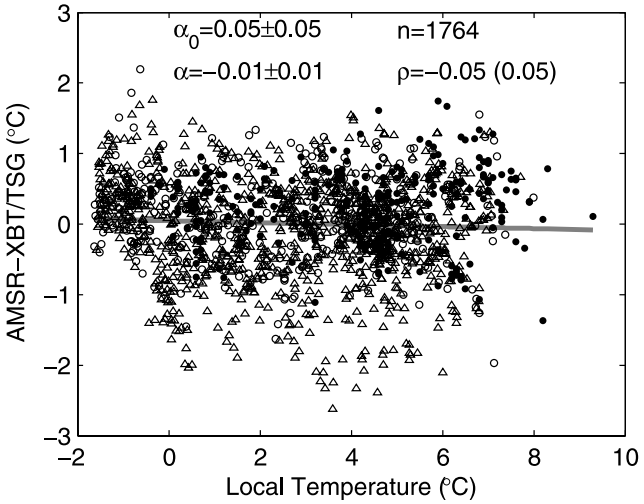

Figure 12. Scatterplots of temperature difference between AMSR-E and XBT/TSG against local temperature. All available data are included (dots for the transects between Hobart and Dumont d'Urville, and circles (XBT) and triangles (TSG) for the Drake Passage transects). The linear regression of ΔSST to local temperature ($\Delta SST = \acute{a}_0 + \acute{a}SST_{xbt}$) is shown as the gray line. The regression coefficients, total number of data (n), and correlation (ñ) between ΔSST and XBT SST are listed in the figure.

[37] We also considered the possibility that ΔSST has either a geographic bias or a temperature dependence. These effects are somewhat difficult to differentiate in the Southern Ocean since temperature varies strongly with latitude. To look at temperature difference as a function of geographic location, we averaged ΔSSTs in 1 degree latitude by 1 degree longitude bins, as indicated by colored dots in Figure 1. No clear relationship is found, although there is some suggestion that ΔSST tends to be positive at the center of the transects south of Australia and more negative at either end. Figure 12 shows the ΔSST as a function of local temperature as measured by the in situ XBT/TSG SST measurements, along with the linear regression of ΔSST to local temperature indicated by the gray line. The dependence of ΔSST on local temperature is marginal, though ΔSST increases at the temperature extremes. The warm bias at low temperature may be due to the effect of unflagged sea ice at the ice edge.

[38] To summarize, our examination indicates that the temperature difference between AMSR-E SST and the SST from XBT/TSG observations is primarily affected by the wind speed and atmospheric water vapor. The value of ΔSST does not depend strongly on cloud liquid water, local time, geographic location, or local temperature. In contrast with previous conclusions that ΔSST diminishes at wind speeds above 6 m s^{-1} [*Donlon et al.*, 1999, 2002; *Gentemann et al.*, 2004], in these Southern Ocean observations ΔSST becomes more negative with increasing wind speed for wind speeds above 6 m s^{-1}. The ΔSST also becomes more negative with increasing atmospheric water vapor. The dependence of ΔSST on wind speed and water vapor suggests that the calibration of the AMSR-E measurements based on in situ observations mostly in the tropics and midlatitudes does not capture all of the relevant processes affecting SST in the Southern Ocean.

[39] To derive a more general relationship between ΔSST, wind speed and water vapor in our study region, we combined all available data together and regressed ΔSST to wind speed and water vapor simultaneously. To account for the seasonal difference as shown in Table 1, we also applied the regression analysis to summer and winter cases separately. The regression coefficients are summarized in Table 2. Table 2 also shows the correlation coefficients of ΔSST with wind speed and water vapor and the number of data. For all cases (summer, winter, and all data), the regression coefficients are significantly different from zero and the correlation coefficients exceed the 95% significance level. The dependence of ΔSST on water vapor does not show a significant seasonal difference, with a regression slope about 0.02 °C mm^{-1} for both summer and winter. However, the dependence of ΔSST on wind speed is stronger during summer (0.08 °C s m^{-1}) than during winter (0.03 °C s m^{-1}). The linear regression for all data indicates positive ΔSSTs for wind speeds less than 10 m s^{-1} and water vapor less than 10 mm. The best fit formula to convert the AMSR-E SST measurements to bulk in situ SSTs takes the form

$$\Delta SST = (-0.06 \pm 0.02)W + (-0.02 \pm 0.01)V + (0.69 \pm 0.15), \quad (1)$$

where W represents wind speed in m s^{-1} and V is water vapor in mm. The regression (1) is derived on the basis of the geographically limited XBT/TSG observations available for this study in Drake Passage and south of Australia, and we caution that it may not be universally applicable to the whole Southern Ocean.

4.5. Comparisons Between MODIS, Reynolds OI, and XBT SST

[40] MODIS SSTs, which in principle provide higher spatial resolution than AMSR-E, could also be used to

Table 2. Results of the Linear Regression of ΔSST to Wind Speed and Water Vapor Simultaneously for Three Cases: Summer Data and Winter Data Separately and All Data Together[a]

	Variable	Summer	Winter	All Data
Slope	α, °C s m^{-1}	−0.077 ± 0.018	−0.026 ± 0.017	−0.057 ± 0.016
	β, °C mm^{-1}	−0.020 ± 0.009	−0.032 ± 0.014	−0.016 ± 0.008
Intercept	α_0, °C	1.13 ± 0.19	0.23 ± 0.21	0.69 ± 0.15
Correlation	ρ_{wind} (95%)	−0.28 (0.06)	−0.09 (0.07)	−0.21 (0.05)
	ρ_{vapor} (95%)	−0.17 (0.06)	−0.16 (0.07)	−0.09 (0.05)
Number of data		931	833	1764

[a]ΔSST = $\alpha_0 + \alpha W + \alpha V$, where W and V represent wind speed in m s^{-1} and water vapor in mm, respectively. The correlation coefficients of ΔSST with wind speed (ρ_{wind}) and water vapor (ρ_{vapor}) are also listed in the table with the 95% significance level in the parentheses. Total number of data in each case is shown in the last row.

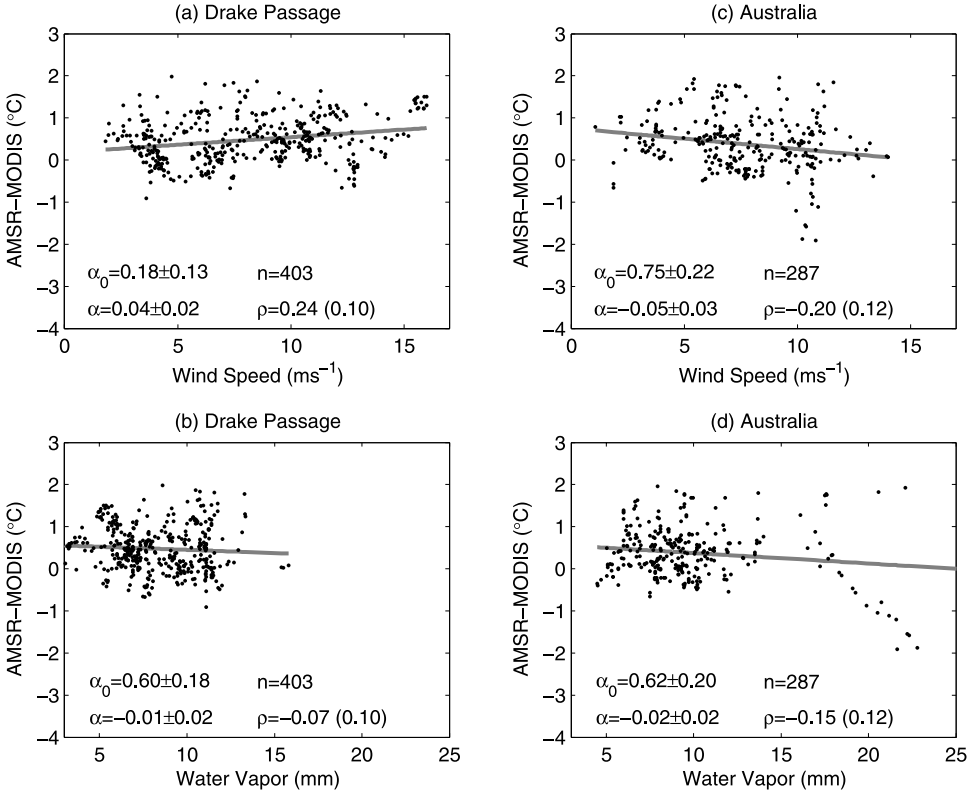

Figure 13. Scatterplots of temperature difference (AMSR-E minus MODIS) against (a) wind speeds and (b) water vapor for the Drake Passage transects. (c, d) Same as Figures 13a and 13b, but for transects between Hobart and Dumont d'Urville. The linear regression of the temperature difference between AMSR-E and MODIS SSTs to wind speed and water vapor is shown by the gray lines.

examine the relationship between the satellite−in situ temperature differences and geophysical parameters. As mentioned in section 3, we found about 300 MODIS observations within a day of the XBT observational times along both sections. However, when we restricted our analysis to observations with wind speeds exceeding 6 m s^{-1} and collected within 5 hours of the in situ XBT observations and removed MODIS data that differed by more than 2°C from XBT, only 45 data points remain. Statistical comparisons between MODIS and XBT SSTs cannot be done with so few data. However, the mean temperature difference between MODIS and XBT SSTs indicates that MODIS SSTs are biased 0.25°C cold in Drake Passage and 0.05°C cold south of Australia. This cold bias may be partly explained by the residual cloud contamination.

[41] Simultaneous measurements from AMSR-E and MODIS can be used to examine how the temperature difference between these two sensors depends on geophysical parameters. As in section 3, we excluded the MODIS data that differ from AMSR-E measurements by more than 2°C. Examination of ΔSST_R (AMSR-E minus MODIS) shows dependence on wind speed (Figures 13a and 13c) for both sections, but with opposite trends: ΔSST_R increases with increasing wind speed at the Drake Passage transect and decreases with increasing wind speed at the transects south of Australia. As shown in Figures 13a and 13c, low-wind-speed data are included in this analysis. Figures 13b and 13d suggest that the temperature difference does not have a statistically significant dependence on water vapor. We also explore the dependence of ΔSST_R on local temperature (derived from XBT observations). Figure 14 shows that ΔSST_R decreases with increasing local temperature. The high ΔSST_R at low local temperature may be partly due to the unflagged sea ice or undetected clouds.

[42] We find that the AMSR-E SSTs are colder than OI SSTs when averaged for the entire Southern Ocean between 30°S and 60°S (not shown). To examine whether the difference is due to a warm bias in OI SSTs, we compare the OI SSTs with in situ observations. Weekly OI SSTs are interpolated to the XBT/TSG locations and times. Scatterplots (Figures 15 and 16) show that, on average, OI SSTs are warmer than XBT/TSG observations for both sections. OI SSTs are 0.51°C and 0.55°C warmer than the XBT observations along transects at Drake Passage and South of Australia, respectively, and are 0.16°C warmer than the TSG observations for the Drake Passage transects. Thus the negative difference between AMSR-E and OI SSTs (section 3) can be explained by the warm bias in the OI SSTs. The temperature difference may be caused by the stratification of the upper ocean during daytime under conditions of low wind speed and high insolation. However, removing daytime and/or low-wind-speed data does not eliminate the warm bias in the OI SST. Examination for winter and summer separately indicates that the warm bias appears during both seasons with stronger biases during summer. This warm bias is inconsistent with the cooler bias found in the Southern Ocean by *Reynolds et al.* [2002]. The inconsistency may reflect differences in the study period.

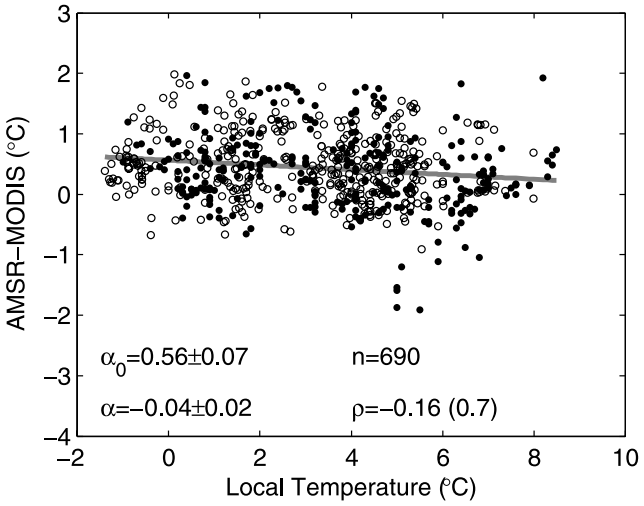

Figure 14. Scatterplots of temperature difference between AMSR-E and MODIS against local temperature (XBT observations). Data from both transects (dots for the transects between Hobart and Dumont d'Urville, and circles for the Drake Passage transects) are included. The linear regression of temperature difference to local temperature ($\Delta SST = \acute{a}_0 + \acute{a}SST_{xbt}$) is shown as the gray line.

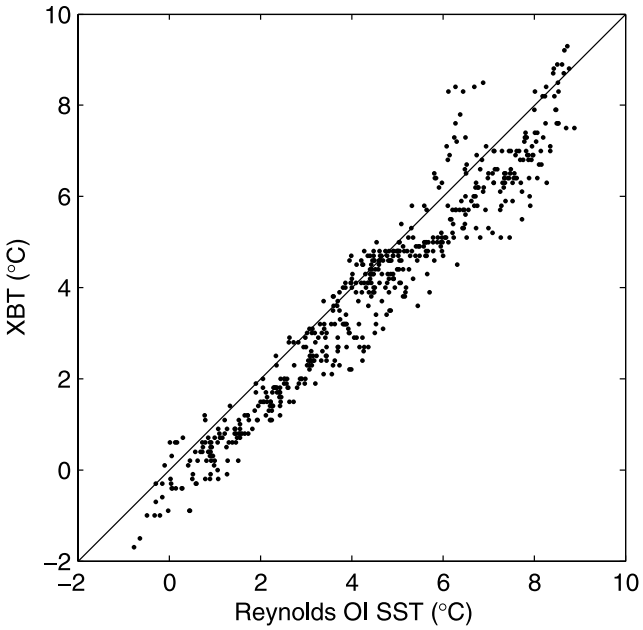

Figure 16. Scatterplot of the XBT measurements against Reynolds OI SST between Hobart and Dumont d'Urville.

Our study are limited to the AMSR-E period (2002–2004), whereas the study of *Reynolds et al.* [2002] are for a longer period from 1982 to 2000.

5. Discussion and Conclusion

[43] Remotely sensed infrared SSTs have become a major data source and are widely used for both oceanographic and atmospheric research. However, cloud contamination has limited the application of infrared SSTs in regions, such as the Southern Ocean, where cloud cover is nearly constant. All-weather measurements from microwave instruments provide an alternative SST data source that have revealed new features at the ocean surface and will significantly improve our understanding of the ocean-atmosphere climate system. Accurate SST products are important in climate studies because SST is a key parameter in the atmospheric and oceanic coupling of heat, gas, and momentum. Accurate estimates of air-sea exchange will depend on remotely sensed products, since in situ observations are sparse in the Southern Ocean. In the past, in situ observations mostly from the tropics and midlatitudes have been used to validate the accuracy of satellite SST retrievals. The validation of microwave SST in the Southern Ocean has not been undertaken before owing to a lack of in situ observations. In this study, we have taken advantage of the XBT/TSG observations along two often repeated sections in the Southern Ocean (Drake Passage and south of Australia) to evaluate the accuracy of SSTs from AMSR-E microwave measurements. Satellite products from MODIS and weekly Reynolds OI were also compared with XBT and AMSR-E SSTs to examine performance of different SST measurements.

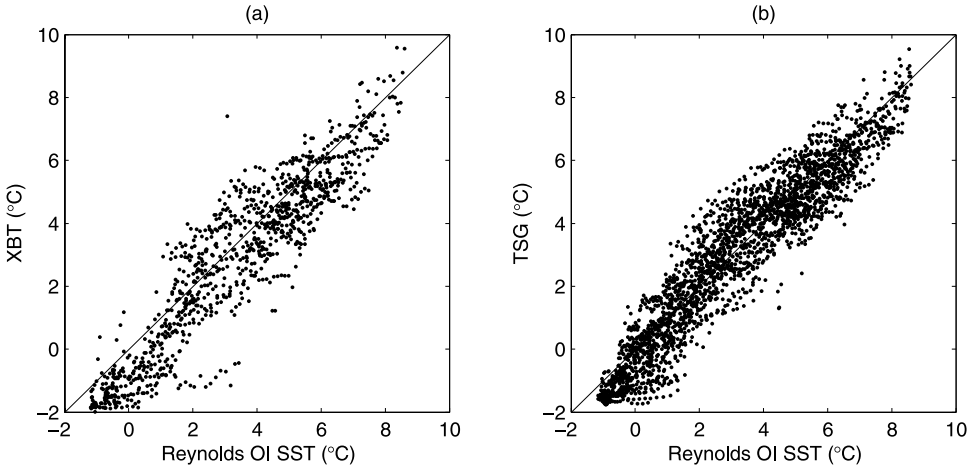

Figure 15. Scatterplots of the (a) XBT against Reynolds OI SST measurements across Drake Passage and (b) TSG against Reynolds OI SST measurements.

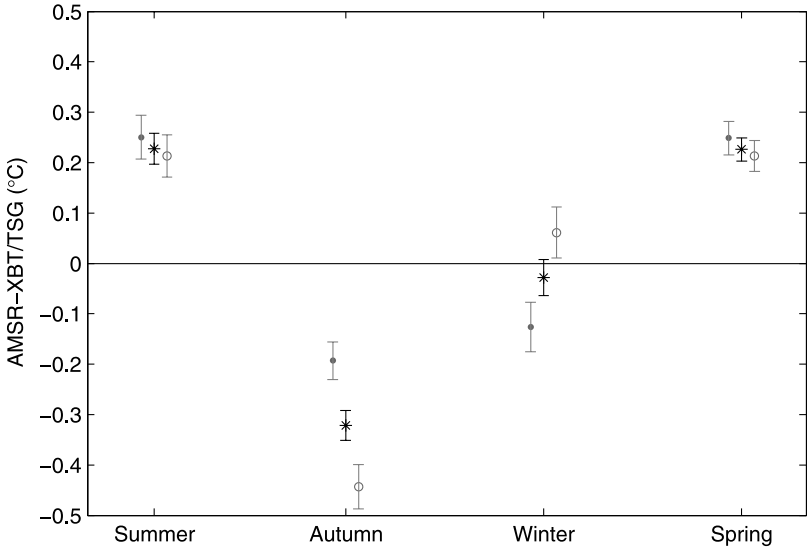

Figure 17. Three-month averaged temperature difference (AMSR minus XBT/TSG) from all data (stars). Dots and circles are the temperature differences for daytime and nighttime ΔSST, separately. The corresponding standard error is indicated by the vertical lines.

[44] XBT SSTs provide the reference in situ temperature for this study, because they are less noisy than TSG measurements. We also find that TSG temperature can be slightly warmer than XBT temperature. Our analysis shows cold biases in MODIS SSTs along both sections compared to XBT and AMSR-E. In contrast with *Reynolds et al.* [2002] who found that OI SSTs have a cold bias in the Southern Hemisphere, our results suggest a warm bias in the OI SST. In comparison with MODIS and OI SSTs, our analysis suggests that AMSR-E provides SST measurements with little bias relative to in situ observations and better temporal coverage.

[45] A strong temperature front is very important to air-sea coupling processes because the largest air-sea heat exchange generally occurs at the temperature front. Our comparison of the Reynolds OI SST with AMSR-E and XBT/TSG temperature fields suggests that the OI SST is too smooth and unable to resolve the narrow temperature fronts in the Southern Ocean. This suggests caution in using the smoothed OI SST in climate studies of the Southern Ocean, as they may influence the nature of the coupling processes. Although MODIS provides SST measurements with higher spatial resolution, near-constant cloud contamination reduces its spatial and temporal coverage.

[46] We confine our comparison of AMSR-E and in situ temperature to measurements collected when wind speeds exceed 6 m s^{-1} for which XBT/TSGs are collected within 5 hours of the AMSR-E overpasses. Overall, AMSR-E SSTs do not show a significant bias (not shown). However, the ΔSST indicates a seasonal difference. As shown in Figure 17, AMSR-E measurements are warmer than in situ observations during spring (October–December) and summer (January–March) and colder during fall (April–June) and winter (July–September). Both daytime and nighttime temperature differences are about 0.23°C during spring and summer. The wintertime temperature difference does not significantly differ from zero. During fall, the AMSR-E SST is 0.32°C colder than XBT/TSG SSTs. Daytime and nighttime ΔSSTs differ during fall and winter (but not during spring and summer) primarily owing to differences between AMSR-E and TSG temperatures.

[47] Even though we have removed low-wind-speed data, we still find that ΔSST becomes more negative with increasing wind speed. The dependence of ΔSST on wind speeds exceeding 6 m s^{-1} indicates that wind speed dependent temperature effects in the Southern Ocean are not eliminated by excluding data with wind speeds less than 6 m s^{-1}, as is appropriate in the tropics [*Donlon et al.*, 2002; *Gentemann et al.*, 2004]. The ΔSST is also related to the atmospheric water vapor: ΔSST becomes more negative with increasing water vapor. This may reflect a sensitivity of the algorithm to low water vapor values that do not occur often at lower latitudes where most of the in situ data were collected and used previously for the AMSR-E SST validations.

[48] The dependence of ΔSST on low wind speed reflects the subskin-bulk temperature difference, whereas the dependence of ΔSST on higher wind speed suggests that the AMSR-E SST retrieval algorithm does not sufficiently account for the wind speed effect in our study region. The dependence of ΔSST on higher wind speeds is consistent with the results of *Wu et al.* [1999] for Geostationary Operational Environmental Satellites (GOES) SST measurements. They found that measurement errors increased at wind speeds higher than 10 m s^{-1}. This high wind speed effect is likely linked to surface roughness, and particularly to the formation of foam and spray at high wind speed. Wind fetch also affects sea surface roughness. The longer wind fetch in the Southern Ocean may give a different relationship between surface roughness and wind speed. Thus the relationship between wind speed and emissivity may be different in the Southern Ocean, which causes a bias in the AMSR-E retrieval of SST.

[49] Our analysis shows that the spatial pattern of the temperature difference between AMSR-E and Reynolds OI is similar to that between AMSR-E and MODIS, which suggests that geophysical parameters, such as the effects of

wind speed effect on microwave emission and cloud contamination on IR measurements, may also contribute to the spatial pattern of the temperature difference.

[50] **Acknowledgment.** This study is supported by NSF grants OPP-0003618 and OPP03-37998, and NASA grant EOS/03-0602-0117.

References

Brisson, A., P. L. Borgne, and A. Marsouin (2002), Results of one year of preoperational production of sea surface temperatures from GOES-8, *J. Atmos. Oceanic Technol.*, *19*, 1638–1652.

Chelton, D. B., F. J. Wentz, C. L. Gentemann, R. A. de Szoeke, and M. G. Schlax (2000), Satellite microwave SST observations of transequatorial tropical instability waves, *Geophys. Res. Lett.*, *27*, 1239–1242.

Ciasto, L. M., and D. W. J. Thompson (2004), North Atlantic atmosphere-ocean interaction on intraseasonal time scales, *J. Clim.*, *17*, 1617–1621.

Donlon, C. J., and GHRSST-PP Science Team (2005), The GHRSST-PP product user manual, GDS-v1.5, report, Int. GHRSST-PP Project Off., Exeter, UK.

Donlon, C. J., T. J. Nightingale, T. Sheasby, J. Turner, I. S. Robinson, and W. J. Emery (1999), Implications of the oceanic thermal skin temperature deviation at high wind speed, *Geophys. Res. Lett.*, *26*, 2505–2508.

Donlon, C. J., P. J. Minnett, C. Gentemann, T. J. Nightingale, I. J. Barton, B. Ward, and M. J. Murray (2002), Toward improved validation of satellite sea surface skin temperature measurements for climate research, *J. Clim.*, *15*, 353–369.

Fairall, C. W., E. F. Bradley, J. S. Godfrey, G. A. Wick, J. B. Edson, and G. S. Young (1996a), Cool-skin and warm-layer effects on sea surface temperature, *J. Geophys. Res.*, *101*, 1295–1308.

Fairall, C. W., E. F. Bradley, D. P. Rogers, J. B. Edson, and G. S. Young (1996b), Bulk parameterization of air-sea fluxes for Tropical Ocean-Global Atmosphere Coupled-Ocean Atmosphere Response Experiment, *J. Geophys. Res.*, *101*, 3747–3764.

Gentemann, C. L., and F. J. Wentz (2001), Satellite microwave SST: Accuracy, comparisons to AVHRR and Reynolds SST, and measurement of diurnal thermocline variability, paper presented at IGARRS, IEEE 2001 International Geoscience and Remote Sensing Symposium, Inst. of Electr. and Electron. Eng., New York.

Gentemann, C. L., C. J. Donlon, A. Stuart-Menteth, and F. J. Wentz (2003), Diurnal signals in satellite sea surface temperature measurements, *Geophys. Res. Lett.*, *30*(3), 1140, doi:10.1029/2002GL016291.

Gentemann, C. L., F. J. Wentz, C. A. Mears, and D. K. Smith (2004), In situ validation of Tropical Rainfall Measuring Mission microwave sea surface temperatures, *J. Geophys. Res.*, *109*, C04021, doi:10.1029/2003JC002092.

Jones, M. S., M. A. Saunders, and T. H. Guymer (1996), Reducing cloud contamination in ATSR averaged sea surface temperature data, *J. Atmos. Oceanic Technol.*, *13*, 492–506.

Latif, M., E. Roeckner, M. Botzet, M. Esch, H. Haak, S. Hagemann, J. Jungclaus, S. Legutke, S. Marsland, and U. Mikolajewicz (2004), Reconstructing, monitoring, and predicting multidecadal-scale changes in the North Atlantic thermohaline circulation with sea surface temperature, *J. Clim.*, *17*, 1605–1614.

McClain, E. P., W. G. Pichel, and C. C. Walton (1985), Comparative performance of AVHRR-based multichannel sea surface temperatures, *J. Geophys. Res.*, *90*, 11,587–11,601.

McPhaden, M. J. (2004), Evolution of the 2002/03 El Niño, *Bull. Am. Meteorol. Soc.*, *85*, 677–695.

Merchant, C. J., and P. L. Borgne (2004), Retrieval of sea surface temperature from space, based on modeling of infrared radiative transfer: capabilities and limitations, *J. Atmos. Oceanic Technol.*, *21*, 1734–1746.

Merchant, C. J., and A. R. Harris (1999), Toward the elimination of bias in satellite retrievals of sea surface temperature: 2. Comparison with in situ measurements, *J. Geophys. Res.*, *104*, 23,579–23,590.

Moore, J. K., M. R. Abbott, and J. G. Richman (1999), Location and dynamics of the Antarctic Polar Front from satellite sea surface temperature data, *J. Geophys. Res.*, *104*, 3059–3073.

Morrow, R., A. Brut, and A. Chaigneau (2003), Seasonal and interannual variations of the upper ocean energetics between Tasmania and Antarctica, *Deep Sea Res., Part I*, *50*, 339–356.

Murray, M. J., M. R. Allen, C. J. Merchant, A. R. Harris, and C. J. Donlon (2000), Direct observations of skin-bulk SST variability, *Geophys. Res. Lett.*, *27*, 1171–1174.

Nalli, N. R., and W. L. Smith (1998), Improved remote sensing of skin temperature using a physical retrieval method, *J. Geophys. Res.*, *103*, 10,527–10,542.

O'Neill, L. W., D. B. Chelton, S. K. Esbensen, and F. J. Wentz (2005), High-resolution satellite measurements of the atmospheric boundary layer response to SST variations along the Agulhas Return Current, *J. Clim.*, *18*, 2706–2726.

Price, J. F., R. A. Weller, and R. Pinkel (1986), Diurnal cycling: Observations and models of the upper ocean response to diurnal heating, cooling and wind mixing, *J. Geophys. Res.*, *91*, 8411–8427.

Reynolds, R. W., N. A. Rayner, T. M. Smith, D. C. Strokes, and W. Wang (2002), An improved in situ and satellite SST analysis for climate, *J. Clim.*, *15*, 1609–1625.

Speer, K., S. R. Rintoul, and B. Sloyan (2000), The diabatic deacon cell, *J. Phys. Oceanogr.*, *30*, 3212–3222.

Sprintall, J. (2003), Seasonal to interannual upper ocean variability in the Drake Passage, *J. Mar. Res.*, *61*, 27–57.

Stammer, D., F. Wentz, and C. Gentemann (2003), Validation of microwave sea surface temperature measurements for climate purposes, *J. Clim.*, *16*, 73–87.

Sutton, R. T., and D. L. R. Hodson (2003), Influence of the ocean on North Atlantic climate variability 1871–1999, *J. Clim.*, *16*, 3296–3313.

Vazquez-Cuervo, J., E. M. Armstrong, and A. Harris (2004), The effect of aerosols and clouds on the retrieval of infrared sea surface temperature, *J. Clim.*, *17*, 3921–3933.

Walton, C. C. (1988), Nonlinear multichannel algorithms for estimating sea surface temperature with AVHRR satellite data, *J. Appl. Meteorol.*, *27*, 115–124.

Wentz, F. J., and T. Meissner (1999), AMSR ocean algorithm, version 2, *RSS Tech. Rep. 121599A*, Remote Sens. Syst., Santa Rosa, Calif.

Wentz, F. J., C. Gentemann, and P. Ashcroft (2003), On-orbit calibration of AMSR-E and the retrieval of ocean products, paper presented at 83rd Annual Meeting, Am. Meteorol. Soc., Long Beach, Calif.

Wick, G. A., W. J. Emery, L. H. Kantha, and P. Schussel (1996), The behavior of the bulk-skin temperature difference under varying wind speed and heat flux, *J. Phys. Oceanogr.*, *26*, 1969–1988.

Wu, X., W. P. Menzel, and G. S. Wade (1999), Estimation of sea surface temperature using GOES-8/9 radiance measurements, *Bull. Am. Meteorol. Soc.*, *80*, 1127–1138.

Xie, S., H. Annamalai, F. A. Schott, and J. P. McCreary (2002), Structure and mechanisms of south Indian Ocean climate variability, *J. Clim.*, *15*, 864–878.

Yoshimori, K., K. Itoh, and Y. Ichioka (1994), Thermal radiative and reflective characteristics of a wind-roughened water surface, J, *Opt. Soc. Am. A Opt. Image Sci.*, *11*, 1886–1893.

S. Dong, S. T. Gille, and J. Sprintall, Scripps Institution of Oceanography, University of California, San Diego, 9500 Gilman Drive, Mail Code 0230, La Jolla, CA 92093-0230, USA. (shdong@ucsd.edu)

C. Gentemann, Remote Sensing Systems, 438 First Street, Suite 200, Santa Rosa, CA 95401-6357, USA.